IL NUOVO CIMENTO Vol. 31 C, N. 4 Luglio-Agosto 2008
DOI 10.1393/ncc/i2009-10314-y

Near-field light emission from semiconductor macroatoms

S. Savasta([1])(*), G. Pistone([1]), O. Di Stefano([1]), G. Martino([1])([2]) and R. Girlanda([1])

([1]) *Dipartimento di Fisica della Materia e Ingegneria Elettronica, Università di Messina Salita Sperone 31, I-98166 Messina, Italy*
([2]) *Dipartimento di Matematica, Università di Messina - Salita Sperone 31 I-98166 Messina, Italy*

(ricevuto il 12 Gennaio 2009; approvato il 15 Gennaio 2009; pubblicato online il 12 Marzo 2009)

Summary. — We present a microscopic theoretical analysis of time and spatially resolved photoluminescence of naturally occurring quantum dots induced by monolayer fluctuations in the thickness of semiconductor quantum wells. In particular we study the carrier dynamics and the emission properties of a semiconductor quantum dot under both continuous-wave and pulsed excitations resonant with the barrier energy levels. We show that collection-mode near-field optical microscopy allows the detection of light emission from excitonic dark states. We find that, at low temperature, the second (dark) energy level displays a carrier density significantly larger than that of the lowest energy level. This behaviour is a consequence of carrier trapping due to the symmetry-induced suppression of radiative recombination.

PACS 68.37.Uv – Near-field scanning microscopy and spectroscopy.
PACS 71.35.-y – Excitons and related phenomena.
PACS 78.67.Hc – Quantum dots.
PACS 78.67.-n – Optical properties of low-dimensional, mesoscopic, and nanoscale materials and structures.

1. – Introduction

One tool frequently used to explore the optical properties of semiconductor nanostructures is photoluminescence spectroscopy (PL). It provides a direct measurement of the optical density of states times the excitonic population density as a function of energy. Detailed simulations of Zimmermann *et al.* [1, 2] have clarified many aspects of the intriguing nonequilibrium dynamics determining the distribution of excitonic populations among the available energy levels in quantum wells (QWs) with interface roughness. Far-field PL spectroscopy provides average measurements over a distribution of different emission sites. The opportunity for important insight is often lost by the inability to resolve finer details within this distribution.

(*) E-mail: ssavasta@unime.it

Scanning near-field optical microscopy (SNOM) has opened the possibility for studying numerous optical phenomena with resolution well below the diffraction limit [3]. It combines the advantages of nanometric resolution of scanning-probe microscopy with the unique possibility of characterizing quantum systems offered by optical spectroscopy. The SNOM ability to resolve the individual quantum constituents of semiconductor nanostructures has been widely demonstrated [4-6].

If the spatial near-field resolution falls below the extension of confined quantum systems, spatially resolved PL maps out the spatial probability distribution of the wave function times the corresponding level occupation [7, 8]. The matrix elements governing the light-matter coupling are a convolution of the quantum states with the exciting electromagnetic field. This convolution implies that exciting a direct gap bulk semiconductor with a light field of a given wave vector resonant with the energy gap results in exciting excitons (*i.e.* bound-state interband optical transitions) within the same wave vector. Succeeding in confining the optical excitation to a very small volume below the diffraction limit, implies the presence of optical fields with high lateral spatial frequencies, determining coupling matrix elements that can differ significantly from far-field ones [8-13]. The most striking manifestation of these effects is the breaking of the usual optical selection rules and the possibility to excite dark states whose optical excitation is forbidden by symmetry in the far field. Spatial maps of dark states in semiconductor nanostructures were simulated for high-resolution SNOM in absorption and two-photon experiments [5, 6, 9, 14]. Moreover, dark states are not able to emit light in the far field, for they generate only fields with high in-plane wave vectors corresponding to evanescent waves. Hence their lifetimes at low temperatures result significantly increased with respect to their bright counterparts.

Here we present recent theoretical results of spatially resolved PL spectroscopy of single macroatoms induced by monolayer fluctuations in the thickness of GaAs/AlGaAs semiconductor quantum wells. We study i) spectral and spatially resolved PL after a far-field continuous wave excitation; ii) time and spatially resolved PL after a far-field pulsed excitation as a function of spatial resolution and temperature.

In particular we investigate the impact of the reduced dark-states relaxation on the distribution of electron-hole pairs among the available energy levels after a far-field continuous wave excitation. We find that this reduced relaxation significantly throws off balance the PL population dynamics resulting in striking deviations from equilibrium. In particular we find that, even at steady state, the occupation of the dark first excited state of a symmetric artificial atom can exceed that of the ground state. Usually larger populations for higher energy levels in nanosystems are observed as consequence of bottleneck effects due to efficient radiative recombination occurring before relaxation to the lowest energy levels. Here the inverted occupations origin from the opposite effect: carrier trapping due to the presence of nonradiative states. While the observation of such effects by means of far-field spectroscopy is prevented (dark states are not able to emit), a SNOM tip can collect the evanescent waves generated by the occupation of dark states. Hence near-field PL reveals to be an excellent laboratory to address general questions regarding nanoscale energy transfer in open quantum systems.

Spatially resolved PL energy spectra do not provide signicant information about the population relaxation dynamics, the linewidths of the resolved individual peaks being related to dephasing rates rather than to population decay-rates. Such information can be gathered by means of near-field spatially and time-resolved PL which offers the possibility to inspect directly the population dynamics of individual quantum states of nanostructured systems.

2. – Theoretical background

In this work we consider quantum states confined in a naturally occurring quantum dot, or terrace, induced by monolayer fluctuations in the thickness of a GaAs/AlGaAs semiconductor quantum well. We adopt the usual envelope function and assume that the electron-hole wave functions factorize into a center of mass (COM) and a relative part given by the $1s$ state of quantum well excitons [1]. We assume that the radiative decay of excitons is not drastically altered by the presence of the SNOM tip. As pointed out in ref. [14], this is a reasonable assumption since the photons can be emitted into any solid-angle direction, and the slightly modified photon density of states in the presence of the SNOM tip is not expected to be of great importance. Within these assumptions, we can write in compact form the near-field PL signal collected by the tip [8]

$$I_{\mathrm{PL}}(\bar{\mathbf{R}}_{\mathrm{out}}, \cdot) = r_0 \sum_{\alpha} \left| o_{\alpha}^{\mathrm{out}}(\bar{\mathbf{R}}_{\mathrm{out}}) \right|^2 \mathcal{F}_{\alpha}(\cdot); \tag{1}$$

where $(\cdot)$ indicates the dependence respectively on ω for spectrally resolved configuration and on t for the time-resolved one. In particular, we have $\mathcal{F}_{\alpha}(\omega) = \mathcal{L}_{\alpha}(\omega)\, N_{\alpha}$ with $\pi \mathcal{L}_{\alpha}(\omega) = \Gamma/[(\omega - \omega_{\alpha})^2 + \Gamma^2]$, where Γ is the dephasing rate of the exciton due to radiative emission and phonon scattering and $\mathcal{F}_{\alpha}(t) = N_{\alpha}(t)$ is the diagonal terms of the exciton density matrix. For a spectrally resolved configuration $o_{\alpha}^{\mathrm{out}} = \int \mathrm{d}^2\mathbf{R}\ \tilde{E}_{\mathrm{out}}(\mathbf{R}) \psi_{\alpha}(\mathbf{R})$ is the overlap of the exciton wave functions with the signal mode $\tilde{E}_{\mathrm{out}}(\mathbf{R})$ supported by the tip centered at the position $\bar{\mathbf{R}}_{\mathrm{out}}$ (collection mode); for a time-resolveved configuration we have instead $o_{\alpha}^{\mathrm{out}} = \int \mathrm{d}^2\mathbf{R}\ g_{\mathrm{out}}(\mathbf{R} - \mathbf{R}_{\mathrm{out}}) \psi_{\alpha}(\mathbf{R})$, g_{out} is the signal supported by the tip centered at the position $\mathbf{R}_{\mathrm{out}}$ (collection mode).

The kinetic equation for the diagonal terms of the exciton density matrix can be derived from the Heisenberg equations of motion for the exciton operators under the influence of the system Hamiltonian [8]. The relevant Hamiltonian is constituted by the bare electronic Hamiltonian of the semiconductor system, the interaction Hamiltonian of the semiconductor with the light field and the interaction Hamiltonian of excitons with the phonon bath. In the following we consider a low-excitation regime, and according to the dynamics-controlled truncation scheme [15] we include only states with one electron-hole pair (excitons). In addition, we neglect the possible coherent phonon states and the memory effects induced by the photon and phonon fields. The obtained set of kinetic equations is [1, 2, 8]

$$\partial_t N_{\alpha} = G_{\alpha} + \sum_{\beta} \gamma_{\alpha \leftarrow \beta} N_{\beta} - 2\Gamma_{\alpha} N_{\alpha}\,, \tag{2}$$

where $\gamma_{\beta \leftarrow \alpha}$ are the acoustic-phonon–assisted scattering rates,

$$\begin{aligned} \gamma_{\beta \leftarrow \alpha} = \frac{2\pi}{\hbar} \sum_{\mathbf{q}} \big((n_{\mathbf{q}} + 1)\, \delta\left(\epsilon_{\beta} + \hbar\omega_{\mathbf{q}} - \omega_{\alpha}\right) \\ + n_{\mathbf{q}} \delta\left(\omega_{\beta} - \hbar\omega_{\mathbf{q}} - \epsilon_{\alpha}\right) \big) \left| t_{\beta\alpha}^{\mathbf{q}} \right|^2, \end{aligned} \tag{3}$$

ω_{α} being the exciton eigenenergies, $\omega_{\mathbf{q}}$ the acoustic phonon dispersion, $n_{\mathbf{q}}$ the phonon thermal occupations described by the Bose function, and $t_{\beta\alpha}^{\mathbf{q}}$ the matrix element for

the exciton-phonon (acoustic) interaction [1]. $2\Gamma_\alpha = r_\alpha + \sum_\beta \gamma_{\beta\leftarrow\alpha}$ is the total out-scattering rate, r_α being the rate for spontaneous emission, proportional to the exciton oscillator strength: $r_\alpha = r_0 |\int \mathrm{d}^2\mathbf{R}\, \psi_\alpha(\mathbf{R})|^2$. The generation rate G_α describes the effect of a light pulse illuminating (possibly locally) the sample: $E_{in} = g_{\mathrm{in}}(\mathbf{R} - \mathbf{R}_{\mathrm{in}})\mathcal{E}(t)$ with $\mathcal{E}(t) = \exp[-i\omega_{\mathrm{in}}t - (t-t_0)^2/4\sigma^2]$. The resulting generation term for the time-resolved configuration is

$$G_\alpha(t) = 2r_0 \left|o_\alpha^{\mathrm{in}}\right|^2 \Im\{\mathcal{E}(t)P_\alpha^*(t)\}\,, \tag{4}$$

with $P_\alpha(t)$ describing the time dependence of the α-th contribution to the excitonic polarization:

$$P_\alpha(t) = e^{-(i\omega_\alpha+\Gamma_\alpha)t} \int_0^t e^{(i\omega_\alpha+\Gamma_\alpha)t'} \mathcal{E}(t')\mathrm{d}t'\,. \tag{5}$$

o_α^{in}, analogously to o_α^{out}, contains the overlap of the exciton wave functions with the signal mode g_{in} delivered by the tip centered at $\mathbf{R}_{\mathrm{in}}$. In collection mode (far-field illumination) the input field can be considered as uniform over the QW plane: $g_{\mathrm{in}}(\mathbf{R}) = \tilde{E}_{\mathrm{in}}^0$. For a continuous wave pumping the generation term depends on the spatial overlap between the illuminating beam and the exciton wave functions:

$$G_\alpha = r_0 \left|o_\alpha^{\mathrm{in}}\right|^2 \mathcal{L}_\alpha(\omega_{\mathrm{in}}) \tag{6}$$

and o_α^{in}, analogously to o_α^{out}, contains the overlap of the exciton wave functions with the signal mode $\tilde{E}_{\mathrm{in}}(\mathbf{R})$ delivered by the tip centered at $\bar{\mathbf{R}}_{\mathrm{in}}$. In collection mode (far-field illumination) the input field can be considered as uniform over the QW plane: $\tilde{E}_{\mathrm{in}}(\mathbf{R}) = \tilde{E}_{\mathrm{in}}^0$.

3. – Numerical results and discussion

3˙1. *Continuous wave pumping.* – We consider quantum states confined in a naturally occurring quantum dot, or terrace, induced by monolayer fluctuations in the thickness of a GaAs/AlGaAs semiconductor quantum well. We adopt the usual envelope function and assume that the electron-hole wave functions factorize into a center of mass (COM) and a relative part given by the 1s state of quantum well excitons [1].

We apply the above-developed theoretical scheme to calculate the individual occupations of exciton states confined in the dot after a continuous-wave far-field optical excitation resonant with the energy of the 1s QW exciton (the dot barrier). The obtained occupations are then used to study the spatially and spectrally resolved (collection mode) light emission from the dot. The effective potential felt by 1s excitons used in our simulations is represented by a sample of (240×240) nm with a prototypical interface-fluctuation confinement of rectangular shape with dimensions (60×90) nm, and monolayer fluctuations giving rise to a 6 meV effective confinement potential. Panels a and b of fig. 1 display the two lowest-energy COM excitonic wave functions $n = 1$ and $n = 2$, respectively. ψ_2 has a node and owing to simmetry has zero radiative decay: $\int \mathrm{d}^2\mathbf{R}\psi_2(\mathbf{R}) = 0$. Of course, it is not an easy task growing perfectly symmetric dots. Nevertheless, it has been recently shown [16] that very strong cancellation effects, almost suppressing the radiative decay, occur also within a realistic heterointerface model

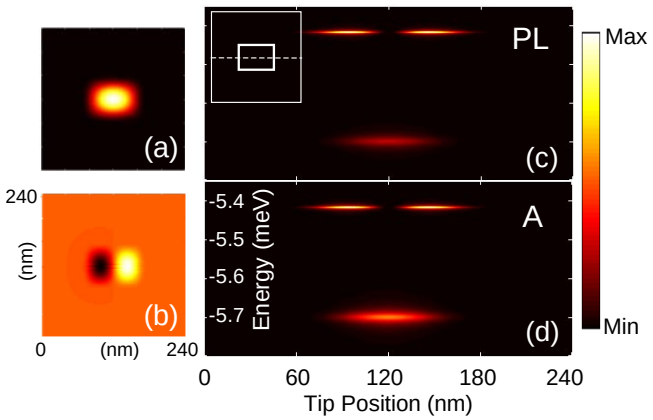

Fig. 1. – (Color on-line) (a) The lowest-energy center-of-mass excitonic wave function and (b) the second energy state. (c) Near-field PL signal (collection-mode) as a function of photon energy and beam position (line scan shown in the inset) obtained under uniform illumination of the sample at the energy of the QW $1s$ exciton. $T = 2\,\mathrm{K}$, FWHM $= 40\,\mathrm{nm}$. (d) Total absorption under local illumination, along the same line, spatial resolution and temperature as in (c).

for excitonic states in growth-interrupted GaAs QWs. Figure 1(c) shows the calculated near-field PL signal as a function of photon energy and beam position obtained after uniform illumination of the sample at the energy of the $1s$ QW exciton in the absence of interface fluctuations, fixed as zero of energy ($\omega_I = 0\,\mathrm{meV}$). The specific line scan is indicated in the inset. A Gaussian profile with FWHM $= 40\,\mathrm{nm}$ of the electromagnetic-mode supported by the collecting tip has been assumed. The line scan clearly evidences the first excited state of the dot which is dark under far-field collection. We observe that its spectral line is more intense and narrow (owing to the absence of radiative decay) than that of the ground state. The calculated PL spectra shows that dark states can be observed by high-resolution SNOM in the usual collection mode configuration after nonresonant far-field excitation, without the need of nonlinear optical interactions. Analogous results are expected for locally collected electroluminescence. Within the proposed experimental configuration, after far-field excitation (or current injection) at higher energy, the dark state get populated by phonon scattering (not forbidden or reduced by the symmetry) and hence produces a corresponding field which can be collected in the near-field (eq. (1)). For comparison we plotted in the lower panel (fig. 1(d)) the total absorption under local illumination (FWHM $= 40\,\mathrm{nm}$). As near-field PL is proportional to this quantity times the level occupations, the comparison provides interesting information about the steady-state exciton populations. The two panels (c) and (d) clearly indicate that the level occupation of the dark state is significantly larger than that of the ground state, at the opposite to what predicted by the Boltzmann distribution. The observed inverted occupations origin from symmetry-suppression of radiative decay of the dark state and the quite small nonradiative scattering at low temperature ($T = 2\,\mathrm{K}$) for states well confined in the dot. Figure 2 shows the calculated level occupations at $T = 2\,\mathrm{K}$ and $T = 30\,\mathrm{K}$. At $T = 2\,\mathrm{K}$ all the occupations with the striking exception of the second energy level decrease monotonically with energy. This level displaying an occupation density which is more than a factor two that of the lowest energy level. At $T = 30\,\mathrm{K}$ the monotonous behaviour is recovered for all the energy levels. We notice that the sum of the occupations obtained at $T = 30\,\mathrm{K}$ is significantly larger than that at

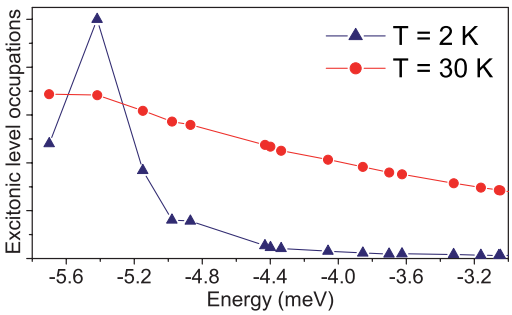

Fig. 2. – (Color on-line) Level occupations (normalized at the maximum) calculated for two different temperatures.

$T = 2\,\mathrm{K}$. At low temperature a large fraction of the resonantly generated QW excitons (with a quite large radiative decay rate) recombine by radiative emission, while at higher temperature phonon scattering lowers this effect, increasing the carrier density captured by the dot. Figure 3 (left panels) shows the near-field (FWHM = 40 nm) PL spectral line scans obtained at three different temperatures. Increasing the temperature all states are able to better thermalize, frequently emitting and absorbing phonons before radiative emission. The influence of spatial resolution on the PL spectral line scans is shown in the right panels of fig. 3. This panels display the line scans calculated at $T = 4\,\mathrm{K}$ for three different spatial resolutions (indicated in the figure). Lowering spatial resolution, the signal from the dark state tend to disappear owing to cancellation effects in the matrix element o_α^{out} governing the light-matter coupling.

3˙2. *Time and spatially resolved photoluminescence.* – We apply the above-developed theoretical framework to calculate the dynamics of excitonic populations after a pulsed

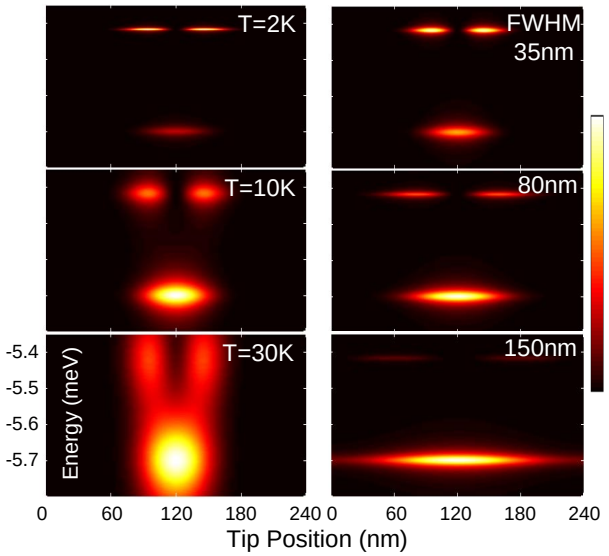

Fig. 3. – (Color on-line) Left: PL spectral line scans calculated at three different temperatures, with FWHM = 40 nm. Right: PL spectral line scans calculated at three different spatial resolutions, at the temperature of 4 K.

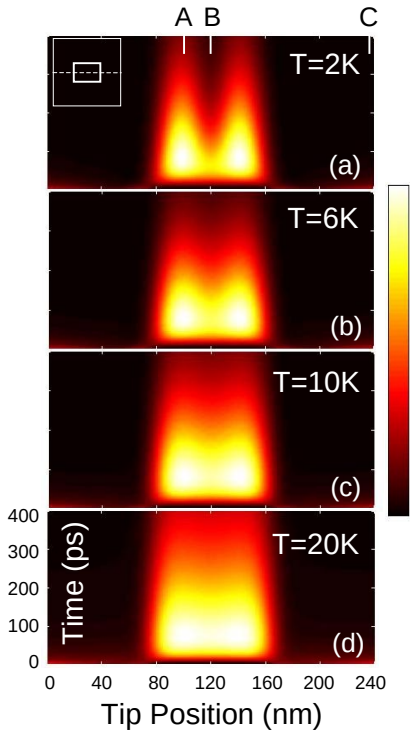

Fig. 4. – Spatially (FWHM = 20 nm in collection mode) and time-resolved PL intensity with fixed $Y = \bar{Y}$ at different temperatures. The specific line scan is indicated in the inset of panel (a).

(FWHM = 1 ps) far-field optical excitation resonant with the energy of the 1s QW exciton (in the absence of momolayer fluctuations). The numerically obtained occupations are then used to study the spatially (collection mode with spatial resolution FWHM = 20 nm) and time-resolved light emission from the dot. The effective potential felt by 1s excitons used in our simulations is represented by a sample of (240×240) nm with a prototypical interface-fluctuation confinement of rectangular shape with dimensions (60×90) nm, and monolayer fluctuations giving rise to a 6 meV effective confinement potential.

Figure 4 shows the calculated spatially and time-resolved PL intensity $I_{\mathrm{PL}}(X, \bar{Y}, t)$ with fixed $Y = \bar{Y}$ for different temperatures. The specific line scan is indicated in the inset of panel (a).

The figure displays a number of interesting features. Inspecting, *e.g.*, panel (a) we can observe the resonant excitation at early times of the dot barrier (the well region around the dot) and its very fast decay due to phonon-assisted relaxation into the dot levels and the corresponding rise of emission from the dot. We also observe that the maximum emission intensity is not located at the dot center but is laterally shifted. This behaviour is a consequence of the fact that the largest contribution to near-field emission at this high spatial resolution comes from the second energy level of the dot that has a p-like shape with a node at the center of the dot. This state, owing to cancellation effects in $o^{\mathrm{out}}_{\alpha=2} = \int \mathrm{d}^2\mathbf{R}\; g_{\mathrm{out}}(\mathbf{R} - \mathbf{R}_{\mathrm{out}})\psi_2(\mathbf{R})$ is dark under far-field collection ($g_{\mathrm{out}} \simeq \mathrm{const}$), but if $g_{\mathrm{out}}(\mathbf{R} - \mathbf{R}_{\mathrm{out}})$ is sufficiently confined as compared to the spatial extension of $\psi_2(\mathbf{R})$, detecting near-field emission from this state becomes possible. Moreover the level occupation of this dark state is larger than that of the first energy state [17], at

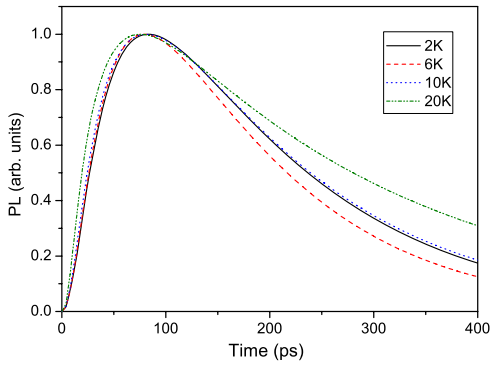

Fig. 5. – Normalized time-resolved PL intensity (FWHM = 20 nm) obtained with the tip position focussed at the dot emission maximum. They are performed fixing the tip in the point $\mathbf{R} \equiv (A, \bar{Y})$ (A is shown in fig. 4(a)) and calculated for the four different temperatures shown in the panels of fig. 4.

the opposite to what predicted by the Boltzmann distribution. The observed inverted occupations origin from the symmetry-suppression of radiative decay of the dark state ($r_2 = 0$) due to cancellation effects [14, 17]. Such interpretation is further confirmed by the fact that the emission from the center of the dot decays before than that from its sides (see fig. 4(a)). Increasing the temperature, we observe a tendency to a more uniform emission from the dot. It is due to the fact that the increase of nonradiative decay with temperature reduces the difference in the total decay rates between the two lowest energy states of the dot. Comparing the panels at different temperatures, we can see, passing from 2 to 6 K, a slightly lowering in the decay time of the dot emission. On the contrary, increasing further the temperature (panels c and d) determines an increase of the decay time. Thus, we find that the temperature behaviour of population decay times strongly differs from that of the excitonic polarization (related to the nondiagonal elements of the density matrix) which monotonically decrease with temperature. This behaviour can be understood as follows: at low temperature only a few energy levels (actually the first two) get populated, when increasing temperature higher energy optically inactive or poorly active levels get populated reducing the overall decay due to radiative recombination. An

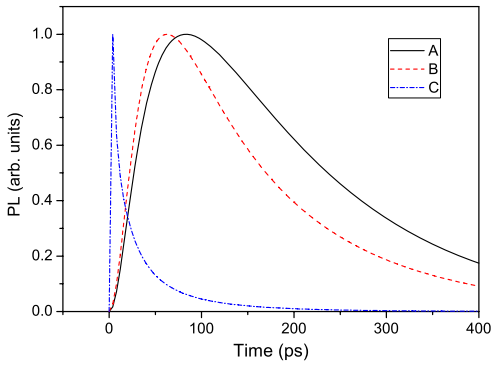

Fig. 6. – Normalized time-resolved PL intensity (FWHM = 20 nm, $T = 2$ K) performed fixing the tip at three different points $(A, \bar{Y}); (B, \bar{Y}); (C, \bar{Y})$ (A-C are shown in fig. 4(a)).

analogous temperature behaviour has been experimentally observed [18]. Further theoretical investigations are needed to confirm this interpretation. This behaviour is better evidenced in fig. 5, which shows the normalized time-resolved PL intensity (obtained with the tip positioned at the dot emission maximum) (A is shown in fig. 4(a)).

Figure 6 compares the normalized time-resolved PL intensities corresponding to the three different tip positions A-C indicated in fig. 4(a). This figure displays data extracted from fig. 4(a) which clarify and confirm the above discussion.

4. – Conclusions

We have theoretically investigated the spatially and time-resolved PL emission of naturally occurring symmetric quantum dots induced by monolayer fluctuations in the thickness of a semiconductor quantum well. The calculated near-field luminescence properties of these states depend critically on tip position, temperature and spatial resolution. The obtained numerical results show that the carrier recombination dynamics is significantly affected by thermal populations in optically inactive or poorly active exciton states in agreement with recent experimental results. The presence of a dark second energy level strongly affects the emission shape at high spatial resolution. The near-field PL calculations here presented clearly indicate the potentiality of time-resolved near-field spectroscopy for addressing general questions regarding nanoscale population dynamics in open nanosystems.

REFERENCES

[1] Zimmermann R. and Runge E., *Phys. Status Solidi (a)*, **164** (1997) 511.
[2] Groβe F. and Zimmermann R., *Superlattices Microstruct.*, **17** (1995) 439.
[3] Courion D., *Near-Field Microscopy and Near-Field Optics* (Imperial College Press, London) 2003.
[4] Savasta S., Martino G. and Girlanda R., *Phys. Rev. B*, **61** (2000) 13852.
[5] Di Stefano O., Savasta S., Martino G. and Girlanda R., *Phys. Rev. B*, **62** (2000) 11071.
[6] Hohenester U., Goldoni G. and Molinari E., *Appl. Phys. Lett.*, **84** (2004) 3963.
[7] Runge E. and Lienau C., *Appl. Phys. B*, **84** (2006) 103.
[8] Pistone G. *et al.*, *Appl. Phys. Lett.*, **84** (2004) 2971.
[9] Mauritz O., Goldoni G., Rossi F. and Molinari E., *Phys. Rev. Lett.*, **82** (1999) 847.
[10] Di Stefano O., Savasta S., Martino G. and Girlanda R., *Appl. Phys. Lett.*, **77** (2000) 2804.
[11] Di Stefano O., Savasta S. and Girlanda R., *J. Appl. Phys.*, **91** (2002) 2302.
[12] Pistone G., Savasta S, Di Stefano O. and Girlanda R., *Phys. Rev. B*, **67** (2003) 153305.
[13] Martino G., Pistone G., Savasta S., Di Stefano O. and Girlanda R., *J. Phys.: Condens. Matter*, **18** (2006) 2367.
[14] Hohenester U., Goldoni G. and Molinari E., *Phys. Rev. Lett.*, **95** (2005) 216802.
[15] Axt V. M., Victor K. and Stahl A., *Phys. Rev. B*, **53** (1996) 7244.
[16] Savona V. and Langbein W., *Phys. Rev. B*, **74** (2006) 075311.
[17] Pistone G. *et al.*, *Phys. Stat. Solidi (c)*, **7** (2008) 2524.
[18] Gurioli M. *et al.*, *Phys. Rev. B*, **73** (2006) 085302.